Biophysical Journal Volume 82 January 2002 481–492

Functional Imaging of Plants: A Nuclear Magnetic Resonance Study of a Cucumber Plant

Tom Scheenen, Anneriet Heemskerk, Andrie de Jager, Frank Vergeldt, and Henk Van As
Laboratory of Biophysics, Department of Agrotechnology and Food Sciences, Wageningen University, Dreijenlaan 3, 6703 HA Wageningen, The Netherlands

ABSTRACT Functional magnetic resonance imaging was used to study transients of biophysical parameters in a cucumber plant in response to environmental changes. Detailed flow imaging experiments showed the location of xylem and phloem in the stem and the response of the following flow characteristics to the imposed environmental changes: the total amount of water, the amount of stationary and flowing water, the linear velocity of the flowing water, and the volume flow. The total measured volume flow through the plant stem was in good agreement with the independently measured water uptake by the roots. A separate analysis of the flow characteristics for two vascular bundles revealed that changes in volume flow of the xylem sap were accounted for by a change in linear-flow velocities in the xylem vessels. Multiple-spin echo experiments revealed two water fractions for different tissues in the plant stem; the spin-spin relaxation time of the larger fraction of parenchyma tissue in the center of the stem and the vascular tissue was down by 17% in the period after cooling the roots of the plant. This could point to an increased water permeability of the tonoplast membrane of the observed cells in this period of quick recovery from severe water loss.

INTRODUCTION

Plant water relations deal with the distribution, movement, and function of water in plant cells, tissues, and organs, the development of internal water deficits and their significance to physiological processes, and how these phenomena are placed in an ecological context (Slatyer, 1967). With the development of new technologies (direct quantification of xylem tension with the xylem pressure probe and detection of air in xylem vessels by cryoscanning electron microscopy), plant water relations are currently one of the most controversial areas in plant physiology (Zimmerman et al., 1993; Canny, 1995; Milburn, 1996; Tyree, 1997). Some important questions are: what is the exact mechanism of water transport in plants? What is the mechanism of embolism repair in xylem vessels? And what is the role (if any) of aquaporins in these mechanisms?

A number of groups have taken efforts in visualizing water transport in plants with nuclear magnetic resonance (NMR). Van As and Schaafsma (1984) and Reinders et al. (1988a, 1988b) used a portable NMR spectrometer (Van As et al., 1994) to measure spatially unresolved xylem water flow in cucumber plants in situ and qualitatively examined the water flow through cut sections of a celery stem with NMR imaging (Schaafsma et al., 1992). Meanwhile, Callaghan et al. (1988, 1994) introduced the combination of static and dynamic NMR microscopy and used it to investigate the origins of contrast in NMR images of biological tissues. Bentrup (1996) indicated the importance of NMR-microscopy to botanists and Chudek and Hunter (1997), and MacFall and Van As (1996) reviewed NMR microscopy as a potentially useful tool in studying plants. After a study of phloem and xylem flow in castor bean seedlings (Köckenberger et al., 1997) it was demonstrated that water transport can be measured localized, and even quantified, in larger plants (Kuchenbrod et al., 1998), as well as in combination with fast imaging techniques to shorten measurement times (Rokitta et al., 1999a; Scheenen et al., 2000a). A recent overview about NMR microscopy in plant science, including both flow/diffusion and anatomy or water density and relaxational behavior applications, was presented by Ishida et al. (2000).

In this paper, we present a quantitative evaluation of temporal changes in different NMR imaging parameters (water fractions, spin-spin relaxation times and flow characteristics of individual pixels and of multiple, added pixels, selected from particular tissues) over a period of several days in a 10-week-old, growing cucumber plant. Water fractions and spin-spin relaxation times (T_2) are obtained by the use of a multiple-spin echo (MSE) train (Edzes et al., 1998). Water fractions and T_2-values of different tissues are interpreted without referring to any "bound" or "free" water, but with a central role for cellular compartment dimensions and exchange over the membranes separating these compartments. Nonimaging studies (Hills and Duce, 1990; Snaar and Van As, 1992b; Hills and Snaar, 1992) already indicated that T_2 could be used to examine membrane permeabilities, which define the exchange rates of water over the cell or tonoplast membrane.

For every pixel, the displacement distribution of water within a certain time is also measured using a pulsed field gradient turbo spin echo (PFG TSE) pulse sequence (Scheenen et al., 2000a), and from this displacement distribution the flow characteristics are calculated as described

Received for publication 4 April 2001 and in final form 27 August 2001.
Address reprint requests to H. Van As, Laboratory of Biophysics, Department of Agrotechnology and Food Sciences, Wageningen University, Dreijenlaan 3, 6703 HA Wageningen, The Netherlands. Tel.: (31)-317-482034; Fax.: (31)-317-482725; E-mail: Henk.VanAs@water.mf.wau.nl

0006-3495/02/01/481/11 $2.00

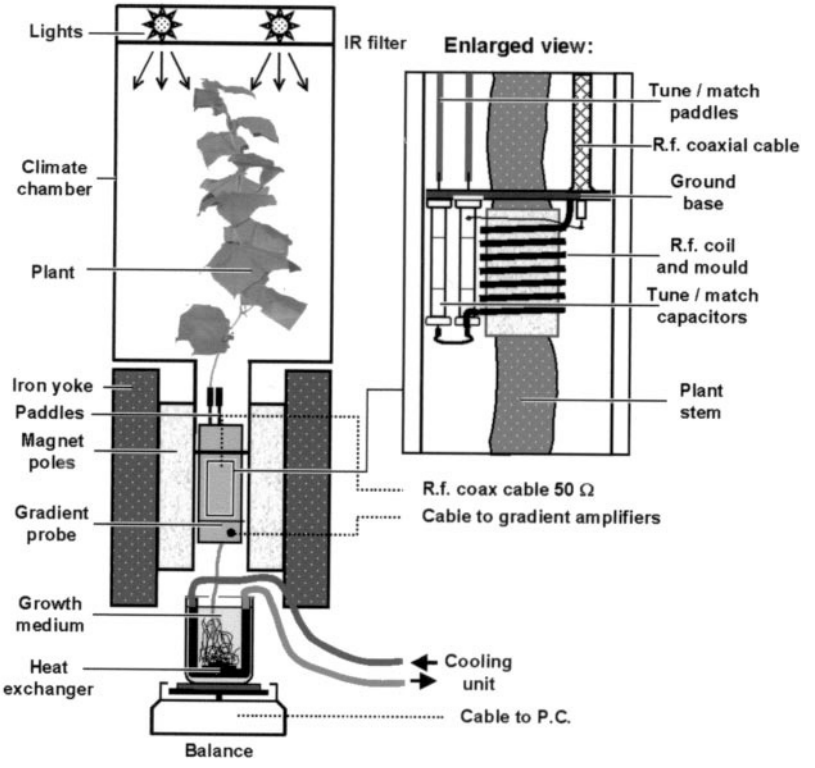

FIGURE 1 Schematic overview of the instrumental setup with the upper part of the cucumber plant in the climate chamber above the electromagnet and the roots in a container with a heat exchanger on the precision balance. The inset shows an enlarged view of the rf coil, wrapped around the stem, in the center of the gradient probe.

by Scheenen et al. (2000b). The total calculated volume flow through the plant stem is compared with the actual uptake of the plant, measured with a precision balance. Changes in water uptake were induced by the normal day/night cycle and a period of cooling the roots of the plant, which has a well known effect of decreasing root permeability and therefore water uptake (Slatyer, 1967; Reinders et al., 1988b).

Imaging of flow and T_2 can relate local changes in biophysical parameters such as flow characteristics (directly) and membrane permeability (indirectly) to controlled changes in environmental conditions. In this way functional information is available with spatial resolution, referred to as "functional imaging."

MATERIALS AND METHODS

Plant material

Two-week-old cucumber seedlings (*Cucumis sativus* L.) were grown in a constantly aerated half-Hoagland solution (Hoagland and Arnon, 1950) in a greenhouse of Unifarm, Wageningen, The Netherlands. The upper 10 cm of the root system grew in an open, cylindrical pod to restrict root-branching within the dimensions of the NMR gradient probe, so later insertion in the gradient probe did not damage the roots. The temperature in the greenhouse was at least 25°C during the day, and 21°C at night. During the photoperiod of 16 h, the plants received direct sunlight and additional light from high-pressure sodium lamps. Under these conditions the plants grew to 2 m in length in ~10 weeks. Flowers were pinched out and occasionally the bottom leaf of the stem was removed with a razor blade to clear the lower 50 cm of the stem before moving the plant from the greenhouse to the NMR imaging setup (removal of the last leaf was at least 4 days before installing the plant).

Instrumental setup

The NMR spectrometer consisted of an SMIS console (SMIS Ltd., Guildford, Surrey, UK), an electromagnet with a 14-cm air gap (Bruker, Karlsruhe, Germany) generating the magnetic field of 0.47 T and an external ^{19}F lock unit (SMIS) stabilizing the magnetic field. A custom-made shielded gradient probe (Doty Scientific, Columbia, SC) with a 45 mm (i.d.) cylindrical bore, accessible from both ends was used. A solenoid radio frequency (rf) coil (diameter 15 mm), which induced and detected the NMR signal, was wrapped around an openable mold, and placed around the plant stem. In <2 min the roots were taken out of the growth solution and put through the 45-mm bore of the gradient probe into an aerated container with identical growing medium. A cooling element inside the container could provide quick cooling of the roots (from 22°C to 3°C in 5 min) and the container itself was placed on a precision balance (LC3201D, Sartorius AG, Göttingen, Germany) below the magnet to monitor water uptake of the plant (Fig. 1). The water uptake, as measured by the balance, was a moving average of 340 s; a single measurement was the mean uptake value in 20 s, every displayed point was the average of 17 measurements. The plant stem and coil mold were fixed inside the gradient probe to fix the position of the plant stem throughout all experiments. The climate chamber above the magnet held the stem and the leaves of the plant at 25 ± 2°C during the photoperiod (from 6 AM to 9 PM, relative humidity 65 ± 5%, illumination ~2×10^2 μmol/m^{2}s (photosynthetic active region), depending on position of the leaves) and at 22 ± 2°C at night. After 4 days in the instrumental setup (growing several cm each day), the roots of the plant in the container were cooled to ~3°C for 3 h, followed by another observation period of 2 days in the setup.

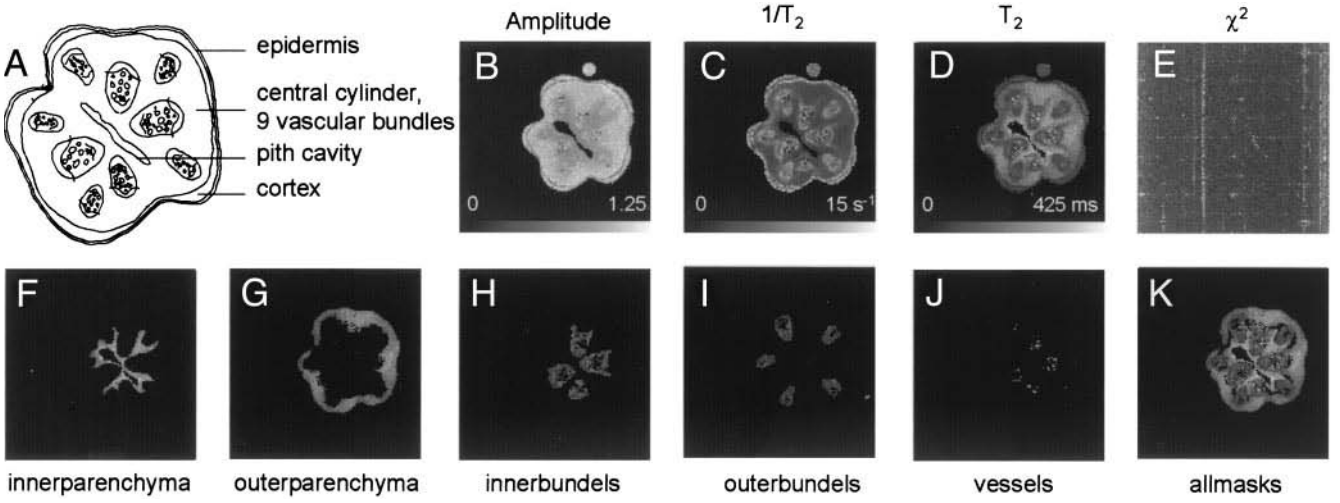

FIGURE 2 NMR images, calculated from one MSE experiment of a cucumber plant. The different tissues in the schematic overview (*A*) of a slice through a cucumber plant stem can clearly be recognized in the R_2 (*C*) and T_2 image (*D*). The amplitude or water density image (*B*) is normalized to the mean intensity of nine pixels in the reference tube. The scale of the color table is somewhat larger than 1.0 because some points in the image may be greater than 1.0 because of noise. Image (*e*) reflects the χ^2 of the monoexponential fit to the decay curve of every pixel. Images (*F–J*) are T_2 images of areas selected with a mask based on amplitude and T_2 value. In image (*K*) all selected areas are combined, leaving some pixels that could not be clearly assigned to a certain tissue. Also, the cortex and the reference tube are not selected in any of the shown masks. Parameters of the NMR experiment: 128 × 128 matrix, field of view 12.8 mm, slice thickness 3 mm, repetition time 3 s, first echo at 6.4 ms, echo time in echo train 4.6 ms, 64 echoes.

NMR imaging pulse sequences

Two different NMR imaging pulse sequences were used to monitor the plant water status and transport: an MSE experiment (Edzes et al., 1998) to evaluate the echo decay of the NMR signal per pixel and a PFG TSE sequence (Scheenen et al., 2000a) to calculate the flow characteristics per pixel (Scheenen et al., 2000b). After the initial slice-selective 90° pulse, both sequences used hard 180° pulses in the spin echo trains to keep interecho intervals short and sample as much of the signal as possible during its decay. The use of a short interecho time, combined with large readout gradients (receiver bandwidth 50 kHz), was necessary to overcome magnetic field inhomogeneities, caused by numerous small air spaces in the plant tissues (Rofe et al., 1995; Donker et al., 1997). Within half the acquisition time of one echo (1.28 ms) the signal decay per pixel attributable to T_2* was negligible and the in-plane resolution was not affected by extra signal attenuation.

In the MSE experiment an echo train was acquired for every step of the phase encode gradient, resulting in an image for every echo in the train. The real part of the phased complex NMR signal $S(t)$ of every pixel in the images in time was characterized by an n exponential decay curve:

$$S(t) = \sum_{i=1}^{n} A_i \exp(-R_{2i}t) \qquad (1)$$

in which A_i is the signal amplitude of fraction i at the moment of excitation ($t = 0$) and R_{2i} is the corresponding relaxation rate ($= 1/T_{2i}$). We used mono- and biexponential fits to extract the biophysical parameters amplitude and relaxation time from different tissues in the cucumber plant stem.

In the PFG TSE experiment (Scheenen et al., 2000a) every individual echo was phase-encoded separately, which shortened the measurement time for one image with a factor equal to the number of echoes used in the TSE train. Displacements of water molecules in the pixels were monitored with two stepped pulsed field gradients in the longitudinal direction (i.e., along the plant stem) with amplitude g, duration δ, and spacing Δ ($\delta < \Delta$), which modulated the complex NMR-signal in amplitude and phase. A Fourier transformation of this signal gave the displacement propagator (Kärger and Heink, 1983) the distribution of displacements of the water molecules within Δ for every pixel in the TSE image. The propagator of stationary water is symmetric around zero displacement (with a Gaussian shape, if the water can diffuse unrestricted), whereas flowing water has a net displacement within the time Δ. The flow characteristics were extracted from the flowing part of every pixel-propagator without assuming any model for the flow-profile within the corresponding pixel, using the NMR signal intensity of a reference tube for calibration (Scheenen et al., 2000b).

In the PFG TSE experiment two different parameter sets were used to obtain either high time or high spatial resolution; a 64 × 64 image matrix with a field of view of 11.0 mm was measured in 21 min (repetition time 2.5 s), whereas a 128 × 128 image matrix with a field of view of 12.8 mm took 42 min of measuring time. The displacement encoding parameters were changed with changing water uptake caused by the day/night cycle (day: 32 g-steps from $-g_{max}$ to $+g_{max-1}$, δ 2.5 ms, Δ 7.0 or 10.0 ms, g_{max} 0.457 to 0.385 T/m; night: δ 2.5 ms, Δ 15.0 ms, g_{max} 0.337 T/m). The matrix size of the MSE experiment was always 128 × 128 pixels with a field of view of 12.8 mm and took 26 min of total acquisition time (repetition time was 3 s). All data processing was performed with IDL (RSI, Boulder, CO).

RESULTS

MSE imaging

Four images were constructed as a result of a monoexponential fit to the NMR-signal decay in the echo train of the MSE experiments (Fig. 2): (*B*) is an amplitude image, representing the fitted amount of water of every pixel in the image; (*C*) an R_2 ($= 1/T_2$) image, characterizing the signal decay rate; (*D*) a T_2 image, revealing better contrast in long T_2-values; and (*E*) a χ^2 image displaying the quality of the fit ($\chi^2 = \sum_{i=1}^{N} (S_i - f_i)^2/(N - 2)$ in which N is the number of echoes and S_i and f_i the value of the ith datapoint and its fitted value). The χ^2 image does not show any intensity

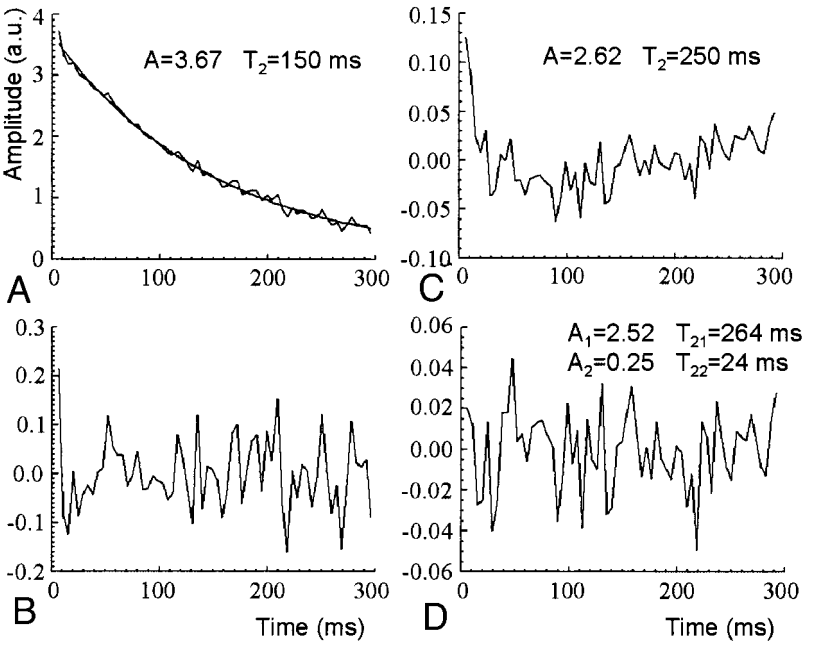

FIGURE 3 Added NMR signal decay curve of pixels in the reference tube and a monoexponential fit to the curve (*A*), the plot of the residuals of the fit to the curve (*B*), and the residuals of a monoexponential (*C*) and a biexponential (*D*) fit to the added signal of all pixels in the inner parenchyma (Fig. 2 *F*). The residuals of the monoexponential fit to the inner parenchyma signal decay is not a straight noisy line, which is the case in the residuals of the biexponential fit. Notice the difference in noise level between (*B*) and (*D*): more pixels could be used in the inner parenchyma signal decay curve, which improves the SNR. Experimental details as in Fig. 2.

related to the anatomy of the stem, indicating no detectable systematic deviations of the data from the monoexponential fit. Fig. 2 *A* is a schematic overview of a transverse slice through a cucumber plant stem. The pixels in the center of the stem with no intensity in the amplitude image correspond with the pith cavity in the stem. The parenchyma in the central cylinder can be divided into inner and outer parenchyma on the basis of a small difference in amplitude (water density), visualized in Fig. 2, *F* and *G*. The central cylinder of the stem generally contains four big and five smaller vascular bundles, which can clearly be distinguished in the R_2 image (Fig. 2, *H* and *I* show T_2 images of the four inner bundles and five outer bundles without xylem vessels, respectively). The tissue in the vascular bundles has T_2-values in the order of 130 ms; large xylem vessels in the bundles are visible with long T_2-values (Fig. 2 *J*; 300 ms). A thin ring, small in amplitude and short in T_2, separates the central cylinder from the cortex. The thin epidermis is visible with high intensity in the R_2 image (T_2 90 ms). The dot above the plant stem is a reference tube filled with an aqueous $MnCl_2$ solution to shorten the T_2 of the water to 150 ms ("doped" water).

As was mentioned earlier, we found no systematic deviations of the data from the monoexponential fit related to the stem anatomy (Fig. 2 *E*). This implies that the signal-to-noise ratio (SNR) of the decay curve of an individual pixel was too low for a meaningful multiexponential fit, although even for an individual pixel, a multiexponential decay is expected because of the different proton pools present in a pixel (water in different cells and/or different cell compartments). Averaging the decays from the pixels of the masks in Fig. 2, *F* to *J* greatly improved the SNR and enabled biexponential fits to the decaying NMR signal. Fig. 3 *A* displays the added NMR-signal decay curve of the pixels in the reference tube and a monoexponential fit to the curve (no partially filled pixels included). A plot of the residuals of the fit shows only noise (Fig. 3 *B*). Because pixels within the reference tube were completely filled with doped water, the calculated amplitude could serve as a 100% water density standard for normalization of the amplitudes. A monoexponential fit to the averaged decay curves of one of the selected areas in the image (the inner parenchyma Fig. 2 *F*) clearly resulted in a systematic deviation from zero in the plot of the residuals (Fig. 3 *C*). In contrast, the plot of the residuals of a biexponential fit to the same data displayed only noise (Fig. 3 *D*); two exponentials described the data well. The mean water density of the inner parenchyma was 75 $\pm$ 2% (total amplitude of the fit compared with the reference tube amplitude), of which (ascribing the two exponentials to two water fractions) a fraction of 9 $\pm$ 1% had a T_2-value of 24 $\pm$ 5 ms and 91 $\pm$ 1% had a T_2 value of 264 $\pm$ 4 ms (shown errors are standard deviations). The tissues in Fig. 2, *F* to *J* were analyzed in the same way, revealing the time course of the water density and corresponding T_2 values of the two water fractions over the course of 3 days, as will be shown later.

Dynamic PFG TSE imaging

Contrary to MSE imaging, in which multiple echoes are used to calculate amplitudes and relaxation times, TSE imaging uses echoes from different refocusing times after excitation to construct an amplitude image. A certain

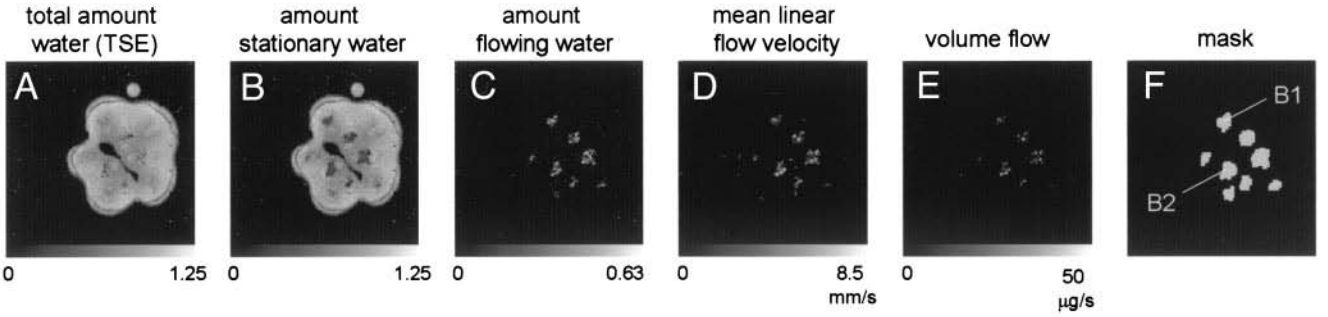

FIGURE 4 NMR images, calculated from a PFG TSE experiment. The total amount of water in the TSE image (*A*) closely resembles the calculated water density image in Fig. 2 *B*. Images (*A–C*) are normalized to the mean intensity of nine pixels in the reference tube (= 1.0). The amount of flowing water can be recalculated in the cross-sectional area of flow for every pixel, assuming that a vessel is homogeneous along the direction of the plant stem over the thickness of the slice (3 mm). Apart from the cross-sectional area of flow, the linear-flow velocity of the flowing water (*D*) and the volume flow (*E*) can be calculated. Image (*F*) indicates the individual vascular bundles as eight gray areas, representing all pixels with flowing water for every bundle. For bundles B1 and B2 the flow characteristics were recalculated with added propagators and studied in more detail. Parameters of the NMR experiment: 128 × 128 matrix with field of view 12.8 mm, repetition time 2.5 s, 32 echoes in TSE train, Δ 14.5 ms, δ 2.5 ms, g_{max} 0.330 T/m.

amount of T_2 weighing is incorporated in the image, as was already mentioned with the introduction of the technique (Hennig et al., 1986). If relaxation times are long, compared with the time from excitation to the first echo that determines the integral of the image (Scheenen et al., 2000a), signal attenuation because of T_2 is small and the TSE image will hardly show any T_2 contrast. With the used time from excitation to the first echo (21 ms), the TSE image of Fig. 4 *A* has only minor deviations from the calculated amplitude image in Fig. 2 *B*; the low amplitude ring between the central cylinder and the cortex with short T_2 has lost some intensity in the TSE image compared with the calculated amplitude image. In both the TSE and MSE image, the inner parenchyma has also lost some intensity because of saturation. The repetition time of the TSE experiment was 2.5 s (3.0 s in MSE) which was not long enough for the protons in the inner parenchyma to return to equilibrium completely (T_1 values might have exceeded 1 s).

Analyzing a PFG TSE experiment as described elsewhere (Scheenen et al., 2000b), we calculated the amount of stationary water (Fig. 4 *B*), the amount of flowing water (Fig. 4 *C*), the mean linear velocity of the flowing water (Fig. 4 *D*) and the volume flow (Fig. 4 *E*) for every pixel in the TSE image. Using the reference tube for calibration, the intensities of Fig. 4, *A–C* represent an amount of water between 0 and 1.0, where 1.0 is the averaged intensity of nine pixels in the reference tube, representing 100% water density. The mean linear-flow velocities of the flowing water in the xylem vessels reached levels up to 8 mm/s, where maximum velocities could exceed 15 mm/s in the center of a vessel. Vessels in 8 of the 9 vascular bundles are visible in Fig. 4 *C*. With the highest volume flow velocities in the vessels of three vascular bundles in the center of the stem, the majority of the water transport in the shown slice of the cucumber plant stem occurred in those three vascular bundles. We set a positive threshold value (~2 × root-mean-square noise level) in the volume flow image to calculate the total water transport through the slice in the plant stem. The total volume flow was a summation of values of those pixels that exceeded the threshold and had at least one neighboring pixel, also with a value above this threshold. The calculated total volume flow through the slice in the plant stem was compared with water uptake values from the balance measurements (see below). The calculation of the flow characteristics could also be performed with a summation of all propagators of one vascular bundle. For two representative vascular bundles B1 and B2, indicated in the mask of all pixels with flowing water for every bundle in Fig. 4 *F*, the changes in flow characteristics in time will be considered in more detail.

The parameters for the PFG TSE experiments were set to measure the xylem flow; the flow-encoding time Δ between the two pulsed field gradients was short (7 to 15 ms), because linear-flow velocities in the xylem were high (locally >15 mm/s). With short Δ-values it is difficult to distinguish displacements of water molecules originating from self-diffusion from displacements of water molecules that flow slowly (e.g., in phloem sieve tubes). This so-called dynamic range problem is illustrated in Fig. 5; the sum of all propagators that show xylem flow has a large shoulder from displacements 0 to 190 μm, whereas the sum of all propagators in phloem regions reveals only a small asymmetry of a Gaussian shape. Merely a qualitative evaluation of phloem flow is possible by subtracting the image representing a displacement of +14 μm from the image representing a displacement of −14 μm, as indicated by I-II in Fig. 5 *B*. This procedure unveils the regions of phloem flow for the measured plant in Fig. 5 *B*; adding all intensities in the phloem regions gives a rough indication of the phloem flow through the slice.

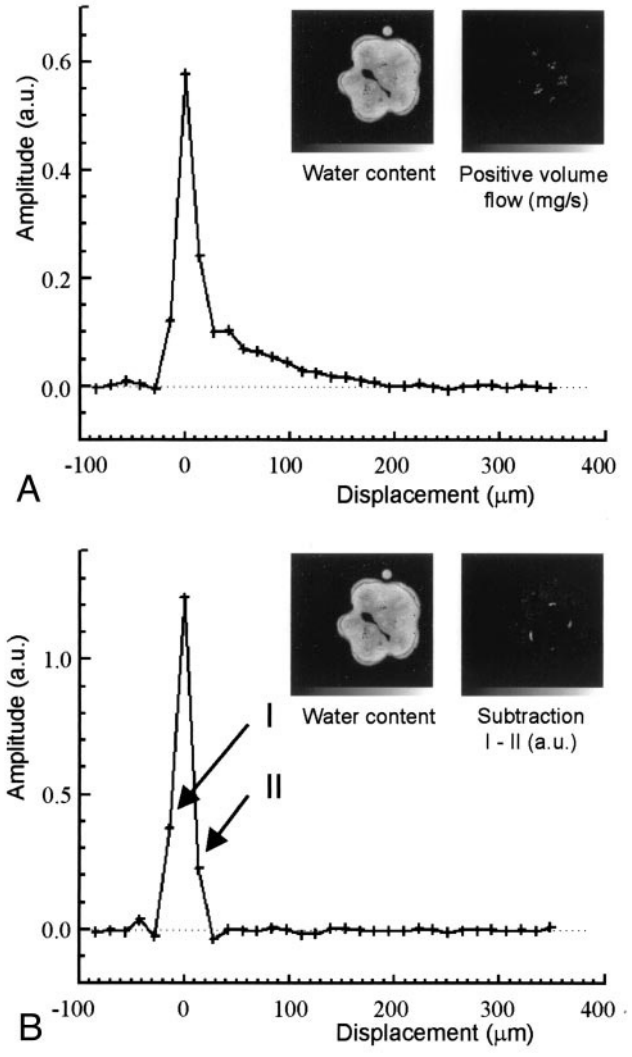

FIGURE 5 The added propagator of all pixels of the image in Fig. 4 that show xylem flow (*A*) and the added propagator of pixels in phloem tissue (*B*). In the inset in (*A*), the images of the calculated water density and volume flow are shown. Subtracting point II from I for every pixel propagator gives an indication of phloem flow as shown in the images in the inset in (*B*). Phloem flow is visible at the periphery of the vascular bundles with a radial symmetry, as can be expected from the bicollateral anatomy of the vascular bundles.

Functional imaging during day/night cycle and root cooling

After 4 days of acclimatization and growth in the experimental setup, the roots of the cucumber plant were cooled rapidly for 3 h. Cooling the roots severely inhibited the uptake of water by the plant, decreasing to levels around nocturnal uptake values before warming up the roots again. An outline of the uptake of the plant from the night before root cooling to 2 days after cooling is presented in the upper part of Fig. 6. The transient response of the plant to turning lights on and off is evident, similar to the reaction to root cooling. Water uptake by the roots was inhibited when the roots were cooled but transpiration of water from the leaves continued, resulting in a net water loss of the plant. The prolonged period of root cooling caused the leaves to wilt and the stomata of the leaves to close (Slatyer, 1967), as shown before in a previous NMR study of a cucumber plant (Reinders et al., 1988b). After warming up the roots, the uptake restored only partially, but with closed stomata of the wilted leaves, water uptake exceeded transpiration and the plant recovered. Within 4 h after warming up the roots again (before the lights were turned off), the plant did not show any visible sign of water deficit anymore. The day after root cooling the uptake was lower than before root cooling. On the last day, shown in Fig. 6, water uptake was almost back to the level before root cooling.

The total volume flow through the imaged slice of the plant, measured with NMR and calculated as indicated earlier, is also plotted in Fig. 6. Again, the response to the day/night cycle and the steep decrease in volume flow as a reaction to root cooling are evident. Moreover, from the start of root cooling to the end of the shown experiment, the calculated NMR data come close to the balance uptake values, so nearly all water that actually flows through the xylem has been localized. Early on the day of root cooling, the calculated NMR flow does not coincide with the high uptake values, measured with the balance. Although the balance measurements in that region are quite noisy or even absent because of too fierce aeration, one can still observe a difference between the balance measurement (~6.5 to 7.0 mg/s) and the calculated NMR flow (~4.5 mg/s) (the reason for this difference will be discussed below). A qualitative evaluation of phloem flow, as described in Fig. 5 *B*, is displayed in the lower part of Fig. 6. The intensity of the phloem flow is in arbitrary units and shows only a reaction to root cooling; any response to the day/night cycle is not clear from the data.

The course of the flow characteristics, calculated for two complete vascular bundles (Fig. 4 *F*), is shown in Fig. 7. The volume flow of the bundles in Fig. 7 *C* resembles the overall uptake of the plant. Bundle B2 (Fig. 4 *F*), indicated with triangles in Fig. 7, transported more than twice the amount of water (0.94 ± 0.02 mg/s (standard error) over the first day after root cooling) than bundle B1, indicated with diamonds in Fig. 7 (0.41 ± 0.02 mg/s (standard error)). Transients in volume flow were a result of changing linear-flow velocities in both vascular bundles. Significant changes in the cross-sectional area of flow are not visible (Fig. 7 *A*, mean cross-sectional area of flow of bundle B1 is 0.16 ± 0.02 mm^2 (standard deviation) over the whole experiment, 0.18 ± 0.03 mm^2 (standard deviation) for bundle B2). The flow characteristics for the other vascular bundles were comparable with the two shown in Fig. 7; the strong reaction of the mean linear-flow velocity to the day/night cycle and to root cooling was responsible for the transients in the volume flow; the SNR of the cross-sec-

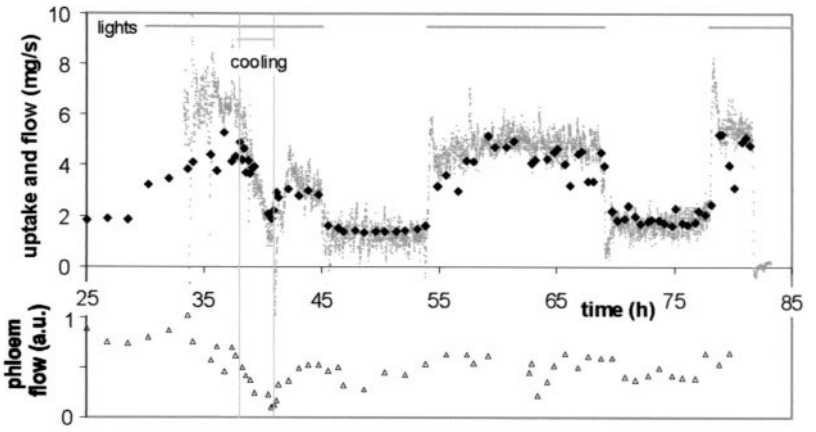

FIGURE 6 The water uptake by the cucumber plant measured with the balance (·) and with PFG TSE NMR (◆). The ground level of evaporation out of the aerated container, visible at the end of the experiment (83 h) when the plant was taken out of the setup, is set to zero. In the lower part of the figure an indication for phloem flow in arbitrary units is plotted (△). The gray lines in the top of the figure indicate the light on periods. The period of root cooling is indicated with two vertical lines. Parameters of the NMR experiments: 128 × 128 matrix with field of view 12.8 mm or 64 × 64 matrix with field of view 11.0 mm, repetition time 2.5 s, 32 echoes in TSE train, Δ, δ, and g were varied with expected flow velocities.

tional area of flow was not high enough to discern a significant change.

For 2 of the 5 selected tissues in Fig. 2, the inner parenchyma and the outer parenchyma, the results of the biexponential fits over the 3 days are shown in Fig. 8. The water fractions of the two components were normalized to the mean intensity of nine pixels in the reference tube. The total water density of the outer parenchyma tissue (the sum of the two water fractions) came close to 1, which can also be seen in the amplitude image, calculated with one exponent in Fig. 2 *B*, where the intensity of the outer parenchyma is as large as the intensity in the reference tube. The total water density of the inner parenchyma tissue was ~0.75–0.80 ($A_1 + A_2$), possibly influenced by partial saturation because of a long T_1, as mentioned before. The two water fractions of the outer parenchyma tissue remained constant throughout the experiment; no influence of the day/night cycle or root cooling could be discerned either in water fraction (Fig. 8 *A*) or in T_2 (Fig. 8 *B*). The amplitude of the large fraction of the inner parenchyma tissue increased ~5% in the last hour of root cooling and the period with the lights on thereafter, which might be because of a decrease in T_1 that cancels the possible partial saturation. The T_2 of this fraction showed a relation with the day/night cycle and with root cooling; with lights off, the T_2 of the fraction was ~0.26 s, dropping to ~0.23 s with the lights turned on, with a steep decrease to ~0.19 s just after the period of root cooling. The T_2 of the smaller fraction of the inner parenchyma tissue did not show a significant dependence on day/night cycle or root cooling. Although the data of the inner and outer vascular bundles (Fig. 2, *H* and *I*) were noisier because of the smaller amount of pixels in that tissue, both tissues showed similar reactions to root cooling; a decrease in T_2 of 15 to 20% of the large water fraction just after the period of root cooling (data not shown).

Fig. 9 recapitulates the results of one MSE and one PFG TSE experiment with a T_2 image and an image with water density and flow information in two directions. The regions of xylem and phloem flow did not overlap, so the spatial in-plane resolution of 100 × 100 μm was high enough to distinguish between the two. Not surprisingly, the vascular bundles with the largest xylem vessels, visible as dots with long relaxation times, showed the largest amounts of water flowing from roots to shoot. Phloem flow was only visible on the exterior side of those bundles that showed the larger quantities of xylem flow.

DISCUSSION

In general, care must be taken in interpreting multiexponential NMR decay curves of plant tissue, because multiexponential relaxation can be caused by cellular inhomogeneity, subcellular compartmentation (Snaar and Van As, 1992a), and the presence of relaxation sinks at the boundaries of (both homogeneous and inhomogeneous) cells or cell compartments (Brownstein and Tarr, 1979; Snaar and Van As, 1992b). However, if an amplitude and T_2 image, although calculated with a monoexponential fit, is used to differentiate between structural tissues, the NMR-signal decay curve of a number of pixels within these tissues can be averaged to increase the SNR, without introducing large cellular inhomogeneities. In homogeneous vacuolized plant tissue, three water fractions have been assigned to different cellular compartments (Hills and Duce, 1990; Snaar and Van As, 1992b; van Dusschoten et al., 1995): the vacuole (large fraction with long T_2), the cytoplasm (small fraction with intermediate T_2), and the cell wall and extracellular water (small fraction with short T_2) (Snaar and Van As, 1992b; van Dusschoten et al., 1995). In this study we fitted the decay curve with a biexponential function because the SNR was too low to extract a third component with acceptable accuracy (other reasons were that the decay curve was cut off before the signal decayed to zero and the first part of the decay curve (time before first echo) was not available). The larger fraction of the two, with the long T_2, can still be assigned to vacuolar water, whereas the small fraction with short T_2 represents water from the cytoplasm and perhaps

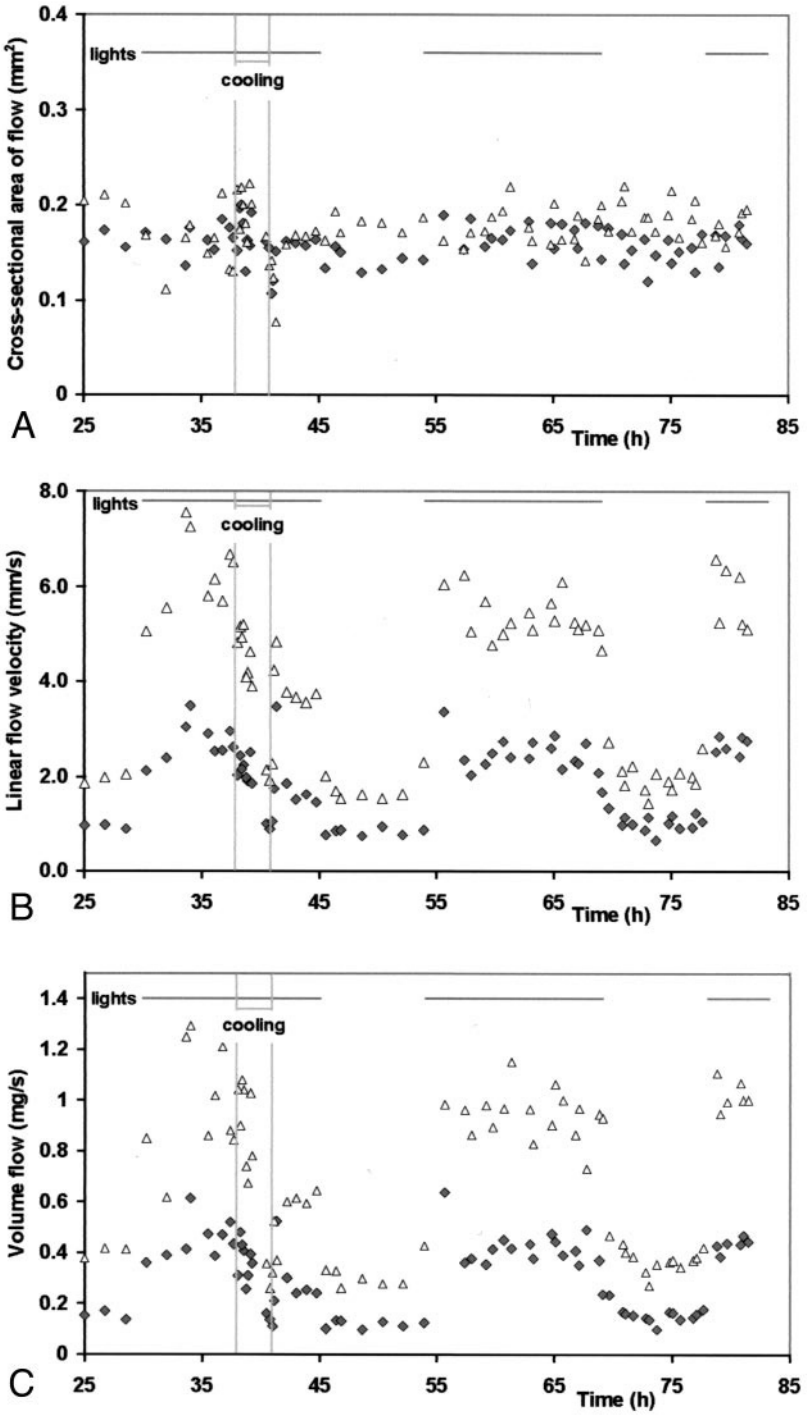

FIGURE 7 The flow characteristics for two vascular bundles, calculated with the summation of all propagators that show flow within one bundle. The cross-sectional area of flow of a bundle in mm^2 (*A*) multiplied with the mean linear-flow velocity of the same bundle in mm/s (*B*) equals the volume flow in mm^3/s or mg/s (*C*). Again, the gray lines in the top of the figure indicate the light on periods and root cooling is indicated with two vertical lines. The diamonds indicate a peripheral vascular bundle (area B1 in Fig. 4 *F*), whereas the triangles indicate one of the four vascular bundles in the center of the stem (area B2 in Fig. 4 *F*).

contributions of water inside the cell wall and extracellular water. The T_2 of the large water fraction is a weighted mean average value of the T_2 of the water in the individual vacuoles, which differ slightly in size and in T_2. Changes in the calculated T_2 can be explained with a model that describes a relation between the observed T_2 of the vacuolar water fraction and the average intrinsic bulk T_2 of the water in the vacuoles, the average surface sink strength density H, and the average dimensions of the vacuoles (Snaar and Van As, 1992b; Donker et al., 1997):

$$1/T_{2,\mathrm{obs}} = H(1/r_x + 1/r_y + 1/r_z) + 1/T_{2,\mathrm{bulk}} \qquad (2)$$

The dimensions of the vacuoles can be expressed in the average radii r_x, r_y, and r_z in three directions. H indicates the rate of magnetization loss at the vacuolar membrane,

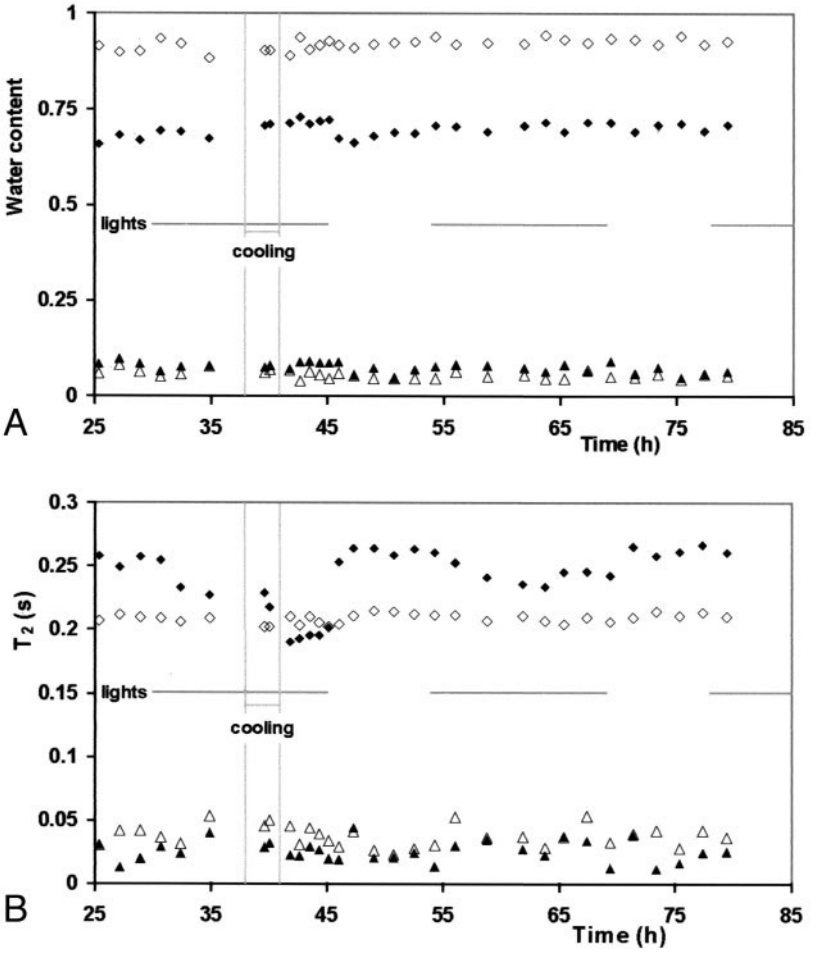

FIGURE 8 The water density (*A*) and corresponding relaxation time T_2 (*B*) for two fractions of the inner parenchyma tissue (♦ and ▲) and the outer parenchyma tissue (◇ and △), calculated with a biexponential fit to the averaged NMR-signal decay of all pixels from the regions indicated in Fig. 2, *F* and *G*.

either because of wall relaxation or exchange of water with the short-T_2 cytoplasm, or even exchange between extracellular water and water in the vacuole (passing through the cytoplasm). The validity of the relation between $1/T_{2,obs}$ and cell dimensions for vacuolized cells has recently been demonstrated for cells in different internodes in the apical zone of maize and pearl millet plants (van der Weerd et al., 2001).

How can this model be used to interpret the dramatic changes in time in the T_2 of the vacuolar water fraction of the inner parenchyma tissue as shown in Fig. 8? The largest change in T_2 is the 17% drop (from 0.23 to 0.19 s) in the 4.5-h period just after root cooling. The time and period in which the T_2 is shorter rules out a temperature effect; the temperature of the roots had already been set back to normal when T_2 values had just dropped. A decrease in stem diameter, as reported by Reinders et al. (1988b), cannot be the cause of the drop either, as the stem diameter is back to the original value within 15 min after cooling. The water density of the vacuolar water fraction increased only ~5% in the period of smaller T_2 values, indicating that the amount of water inside the vacuoles hardly changed, and moreover, that the volume of the vacuoles (r_x, r_y, and r_z) remained constant within 5%. The vacuoles are not likely to accumulate large amounts of paramagnetic ions, which would lower the value for $T_{2,bulk}$, simply because these ions are not present in substantial amounts. The only variable that can be responsible for the 17% decrease in T_2 is H.

The increase in H, the rate of magnetization loss over the vacuolar membrane, might indicate an increase in exchange speed of water between the cytoplasm and the vacuole, or an increase in the tonoplast permeability for water. More protons from water, crossing the vacuolar membrane, lose their magnetization in the cytoplasm and, if the distance from tonoplast membrane to cellular membrane is small (in the order of 1 μm), in the cell wall. In this way, even a change in plasmalemma membrane permeability could affect H and, thereby, also $1/T_{2,obs}$.

The two water fractions in the outer parenchyma tissue did not show any changes in water density and T_2 over the studied period of time, contrary to the inner parenchyma tissue and the tissue in the inner and outer bundles that all clearly showed a decrease in T_2 of the large (vacuolar) water fraction. In the period after root cooling, in which the plant recovered from severe water loss, the decrease in T_2 in tissue around xylem vessels and tissue in the inner paren-

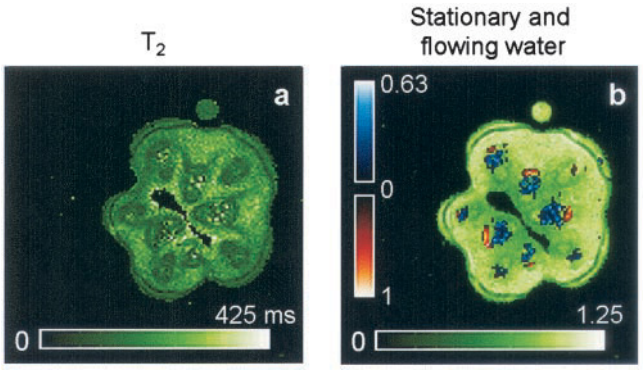

FIGURE 9 Two images summarizing an MSE and a PFG TSE experiment. The image in (*a*) is the T_2 image from Fig. 2 *D*. The image in (*b*) is an image of the water density (Fig. 4 *A*), overlaid with an image of the amount of water flowing upwards in the xylem (Fig. 4 *C*) and an image with a qualitative indication of phloem flow (*inset* in Fig. 5 *B*). The green color scale in (*b*) represents the total amount of water, whereas the blue color scale represents the amount of flowing water, both relative to the average intensity of nine pixels in the reference tube (= 1). The red color scale indicates phloem flow intensity qualitatively, in arbitrary units.

chyma indicates an increase in *H*, which in turn could mean an increase in tonoplast and/or cell membrane permeability, important for restoring the water balance of the plant. Of course, this hypothesis needs to be tested further.

Generally, the total water uptake in Fig. 6, calculated from the PFG TSE data, comes close to the water uptake values, measured with the precision balance, although before cooling the roots, the NMR-values were too low. A reason for calculating systematically deviating volume flow values can be found in the presence of vessels with too-high linear-flow velocities, which results in large maximum displacements within Δ. The surface of the flowing part of the pixel-propagator represents the amount of flowing water (Scheenen et al., 2000b, Fig. 5 *A*). A large maximum displacement at a given amount of flowing water stretches the pixel-propagator all over the displacement axis, lowering the amplitude into the noise, where it can not be quantified anymore. Solutions for this problem are presented elsewhere (Scheenen et al., in preparation).

The flow characteristics of the complete individual vascular bundles in the experiment, as shown by two representative bundles in Fig. 7, reveal the development of the cross-sectional area of flow, the mean linear-flow velocity and the volume flow in absolute quantities. The difference in cross-sectional area of flow for the two bundles is small (0.18 ± 0.03 (SD) $- 0.16 \pm 0.02$ (SD) mm^2), whereas the difference in volume flow (and mean linear-flow velocity) is more than a factor of 2 (0.94 ± 0.02 (SE) to 0.41 ± 0.02 (SE) mg/s). Assuming an equal pressure difference over the two bundles, the volume flow through a circular tube or vessel is related to the fourth power of the vessel radius (the Hagen-Poiseuille law (Bird et al., 1960)). Therefore, the bundle with the higher flow rates must have more vessels with larger diameters and less vessels with smaller diameters than the other bundle to keep the cross-sectional areas (almost) equal. From Fig. 7 *A* one can not conclude that the period of root cooling had a structural effect on the cross-sectional area of flow; changes in the volume flow rate are accounted for by the linear-flow velocities.

It is difficult to discern extremely slow flow from stationary water when using short Δ values. Although phloem flow has been visualized qualitatively, a quantitative evaluation requires long Δ values. With these long observation times, severe signal loss between excitation and detection of the first echo needs to be avoided. For this purpose it is more appropriate to use a stimulated echo version of the PFG TSE technique (Scheenen et al., 2001), or another flow-sensitive NMR imaging pulse sequence that uses a stimulated echo (Rokitta et al., 1999b).

The overlay image in Fig. 9 *b* suggests that xylem flow and phloem flow are correlated; those vascular bundles that are most active in xylem transport, also take care for the majority of phloem transport. Münch (1930) already proposed that the surplus of water from arriving phloem sap that had originally transported solutes can be released in the xylem to be transported back toward the leaves. Whether this implies a positive correlation between xylem and phloem flow has to be investigated further.

The presented study describes the results of one cucumber plant. Three other investigated plants (data not shown), differing slightly in size and age, displayed similar reactions to root cooling and the day/night cycle concerning water loss of the plant, changes in xylem flow, and T_2. In larger plants with larger water uptake values, again the volume flow rates, calculated from the NMR measurements, were systematically lower than uptake values measured with the balance, especially at high linear-flow velocities. However, comparable patterns in calculated volume flow and measured water uptake were observed during day/night cycle and root cooling periods. In one larger plant, phloem flow could be discerned on the interior and exterior sides of three large vascular bundles in the center of the stem and on the exterior side in four other bundles. In this plant, phloem flow was clearly more intense at night than during daytime, again being the smallest as the roots were cooled.

Functional magnetic resonance imaging (MRI) in plants, as demonstrated here, is a unique tool to study plant responses to different water-availability conditions, cold treatment, or other biotic and abiotic stressors. Post-genomic studies of (genetically modified or wild type) plants with functional MRI could reveal the functionality of gene expression at cell, organ, and whole plant level in water-related processes which are crucial for plant function. Another application could be the induction and refilling of air embolisms in plants to study possible mechanisms behind refilling. Changes in total amount of water, amount of flowing water, amount of stationary water, volume flow, and T_2 can be studied on the tissue

or even single vessel or pixel level. If functional MRI is combined with other techniques, e.g., the xylem pressure probe, one could study xylem pressure and xylem flow at the same time to validate or disaffirm current hypotheses in plant water relations.

CONCLUSION

The combination of T_2 and detailed flow-imaging experiments revealed the functioning of plants in response to environmental changes by tracing water transport in xylem and phloem and the spin-spin relaxation time T_2. The analysis of the MSE experiments, aided by image-guided tissue differentiation, with a biexponential decay curve reproducibly revealed two water fractions for several tissues. The T_2 of the large fraction can be assigned to vacuolar water. A decrease of the T_2 of the vacuolar water fraction of the inner parenchyma tissue and the vascular tissue surrounding the xylem vessels after a period of cooling the roots can be attributed to an increase in the surface sink strength density. This increase in H in the period in which the cucumber plant recovers from severe water loss most probably indicates an increased permeability for water of the tonoplast (and plasmalemma) membrane.

Water transport through the xylem vessels is localized and quantified with the flow imaging experiments, indicating, apart from a normal day/night cycle, a large drop in water uptake of the cucumber plant when the roots are cooled. Because the NMR quantification of flow in the xylem vessels matched uptake values, measured with a balance, it is now possible to study water transport separately in every vascular bundle, and even individually for large xylem vessels. Although the presented flow imaging experiments were optimal to measure the xylem flow, phloem flow could also be discerned. A day/night cycle in phloem flow was not found, but the reaction to root cooling was unambiguous: phloem flow dropped during and just after the period of root cooling. The application of the two imaging techniques to other plants and the study of individual xylem vessels and surrounding tissues in the cucumber plants are two promising aspects for the near future.

This research was supported by the Dutch Technology Foundation STW, applied science division of NWO (project WBI 3493).

REFERENCES

Bentrup, F. W. 1996. NMR-microscopy: observing xylem and phloem conduits at work. *Bot. Acta.* 109:177–179.

Bird, R. B., W. E. Stewart, and E. N. Lightfoot. 1960. Transport Phenomena. John Wiley and Sons, New York.

Brownstein, K. R., and C. E. Tarr. 1979. Importance of classical diffusion in NMR studies of water in biological cells. *Phys. Rev. A.* 19: 2446–2453.

Callaghan, P. T., C. J. Clark, and L. C. Forde. 1994. Use of static and dynamic NMR microscopy to investigate the origins of contrast in images of biological tissues. *Biophys. Chem.* 50:225–235.

Callaghan, P. T., C. D. Eccles, and Y. Xia. 1988. NMR microscopy of dynamic displacements: k-space and q-space imaging. *J. Phys. E. Sci. Instrum.* 21:820–822.

Canny, M. J. 1995. A new theory for the ascent of sap-cohesion supported by tissue pressure. *Ann. Bot.* 75:343–357.

Chudek, J. A., and G. Hunter. 1997. Magnetic resonance imaging of plants. *Prog. Nucl. Magn. Reson. Spectrosc.* 1:43–62.

Donker, H. C., H. Van As, H. J. Snijder, and H. T. Edzes. 1997. Quantitative ^{1}H-NMR imaging of water in white button mushrooms (*Agaricus bisporus*). *Magn. Reson. Imaging.* 15:113–121.

Edzes, H. T., D. van Dusschoten, and H. Van As. 1998. Quantitative T_2 imaging of plant tissues by means of multi-echo MRI microscopy. *Magn. Reson. Imaging.* 16:185–196.

Hennig, J., A. Nauerth, and H. Friedburg. 1986. RARE imaging: a fast imaging method for clinical MR. *Magn. Reson. Med.* 3:823–833.

Hills, B. P., and S. L. Duce. 1990. The influence of chemical and diffusive exchange on water proton transverse relaxation in plant tissues. *Magn. Reson. Imaging.* 8:321–332.

Hills, B. P., and J. E. M. Snaar. 1992. Dynamic q space microscopy of cellular tissue. *Mol. Physiol.* 76:979–994.

Hoagland, D. R., and D. I. Arnon. 1950. The water-culture method for growing plants without soil. *Calif. Agric. Exp. St. Circ.* 347.

Ishida, N., M. Koizumi, and H. Kano. 2000. The NMR microscope: a unique and promising tool for plant science. *Ann. Bot.* 86:259–278.

Kärger, J., and W. Heink. 1983. The propagator representation of molecular transport in microporous crystallites. *J. Magn. Reson.* 51:1–7.

Köckenberger, W., J. M. Pope, Y. Xia, K. R. Jeffrey, E. Komor, and P. T. Callaghan. 1997. A non-invasive measurement of phloem and xylem water flow in castor bean seedlings by nuclear magnetic resonance microimaging. *Planta.* 201:53–63.

Kuchenbrod, E., E. Kahler, F. Thurmer, R. Deichmann, U. Zimmermann, and A. Haase. 1998. Functional magnetic resonance imaging in intact plants: quantitative observation of flow in plant vessels. *Magn. Reson. Imaging.* 16:331–338.

MacFall, J. S., and H. Van As. 1996. Magnetic resonance imaging of plants. *In* Nuclear Magnetic Resonance in Plant Biology. Y. Shachar-Hill and P. E. Pfeffer, editors. The American Society of Plant Biologists, Rockville, Maryland. 33–76.

Milburn, J. A. 1996. Sap ascent in vascular plants: challengers to the cohesion theory ignore the significance of immature xylem and the recycling of Munch water. *Ann. Bot.* 78:399–407.

Münch, E. 1930. Die Stoffbewegungen in der Pflanze. Fischer, Jena, Germany.

Reinders, J. E., H. Van As, T. J. Schaafsma, P. A. de Jager, and D. W. Sheriff. 1988a. Water balance in *Cucumis* plants, measured by nuclear magnetic resonance, I. *J. Exp. Bot.* 39:1199–1210.

Reinders, J. E., H. Van As, T. J. Schaafsma, and D. W. Sheriff. 1988b. Water balance in *Cucumis* plants, measured by nuclear magnetic resonance, II. *J. Exp. Bot.* 39:1211–1220.

Rofe, C. J., J. Van Noort, P. J. Back, and P. T. Callaghan. 1995. NMR microscopy using large, pulsed magnetic-field gradients. *J. Magn. Reson. B.* 108:125–136.

Rokitta, M., A. D. Peuke, U. Zimmermann, and A. Haase. 1999a. Dynamic studies of phloem and xylem flow in fully differentiated plants by fast nuclear-magnetic-resonance microimaging. *Protoplasma.* 209:126–131.

Rokitta, M., U. Zimmermann, and A. Haase. 1999b. Fast NMR flow measurements in plants using FLASH imaging. *J. Magn. Reson.* 137: 29–32.

Schaafsma, T. J., H. Van As, W. D. Palstra, J. E. Snaar, and P. A. de Jager. 1992. Quantitative measurement and imaging of transport processes in plants and porous media by ^{1}H NMR. *Magn. Reson. Imaging.* 10: 827–836.

Scheenen, T. W., D. van Dusschoten, P. A. de Jager, and H. Van As. 2000a. Microscopic displacement imaging with pulsed field gradient turbo spin-echo NMR. *J. Magn. Reson.* 142:207–215.

Scheenen, T. W. J., D. van Dusschoten, P. A. de Jager, and H. Van As. 2000b. Quantification of water transport in plants with NMR imaging. *J. Exp. Bot.* 51:1751–1759.

Scheenen, T. W. J., F. J. Vergeldt, C. W. Windt, P. A. de Jager, and H. Van As. 2001. Microscopic imaging of slow flow and diffusion: a pulsed field gradient stimulated echo sequence combined with turbo spin-echo imaging. *J. Magn. Reson.* 151:94–100.

Slatyer, R. O. 1967. Plant-Water Relationships. Academic Press, London.

Snaar, J. E., and H. Van As. 1992a. A method for the simultaneous measurement of NMR spin-lattice and spin-spin relaxation times in compartmentalized systems. *J. Magn. Reson.* 99:139–148.

Snaar, J. E., and H. Van As. 1992b. Probing water compartment and membrane permeability in plant cells by proton NMR relaxation measurements. *Biophys. J.* 63:1654–1658.

Tyree, M. T. 1997. The cohesion-tension theory of sap ascent: current controversies. *J. Exp. Bot.* 48:1753–1765.

Van As, H., and T. J. Schaafsma. 1984. Noninvasive measurement of plant water flow by nuclear magnetic resonance. *Biophys. J.* 45:469–472.

Van As, H., J. E. Reijnders, P. A. de Jager, P. A. van de Sanden, and T. J. Schaafsma. 1994. In situ plant water balance studies using a portable NMR spectrometer. *J. Exp. Bot.* 45:61–67.

van Dusschoten, D., P. A. de Jager, and H. Van As. 1995. Extracting diffusion constants from echo-time-dependent PFG NMR data using relaxation-time information. *J. Magn. Reson. A.* 116:22–28.

van der Weerd, L., M. M. Claessens, T. Ruttink, F. J. Vergeldt, T. J. Schaafsma, and H. Van As. 2001. Quantitative NMR microscopy of osmotic stress responses in maize and pearl millet. *J. Exp. Bot.* In press.

Zimmerman, U., A. Haase, D. Langbein, and F. Meinzer. 1993. Mechanisms of long-distance water transport in plants: a re-examination of some paradigms in the light of new evidence. *Philos. Trans. R. Soc. Lond. Ser. B.* 341:19–31.